https://doi.org/10.5194/egusphere-2024-2569
Preprint. Discussion started: 25 September 2024

Ground penetrating radar on Rutor temperate glacier supported by ice-thickness modeling algorithms for bedrock detection

Andrea Vergnano[1], Diego Franco[1], and Alberto Godio[1]

[1]Department of Environment, Land and Infrastructure Engineering (DIATI), Politecnico di Torino, Torino, Italy

Correspondence: Andrea Vergnano (andrea.vergnano@polito.it)

Abstract.

The glaciers situated in temperate mountain chains often contain a great percentage of temperate ice, which is ice at the temperature-pressure melting point. They may also contain cold ice, but in smaller percentages and located in the coldest parts of the glacier. Measuring the glacier ice thickness is often carried out with Ground Penetrating Radar (GPR), able to scan ice hundreds of meters thick. Unfortunately, the meltwater contained in temperate glaciers challenges the detection of the ice-bedrock interface with the radar technology, due to signal scattering. According to the literature, only from 12% to 69% of GPR traces have been able to depict the ice-bedrock interface in Swiss glaciers, the percentage varying according to the glacier and the GPR antenna. Besides, GPR data are acquired on straight lines and do not cover the entire glacier area with a fine resolution. These problems affected previous GPR surveys of the Rutor Glacier (Aosta Valley, Southern Europe Alps), reporting an irrealistic, too low, ice thickness. To obtain a more reliable interpretation of the GPR data, estimations from ice-thickness modeling algorithms are employed to guide the analyst in the interpretation of scattered GPR data. Two new GPR datasets of the Rutor Glacier are analyzed, helicopter-based and ground-based. We tested three open-source modeling algorithms that estimate the ice thickness based on the surface topography: GlabTop2 (Glacier Bed Topography), GlaTE (Glacier Thickness Estimation), and OGGM (Open Global Glacier Model). The ice thickness raster maps produced with these models are sampled to extract ice thickness profiles coincident with the GPR measurements. The ice-bedrock interface of GPR profiles is then manually picked, using the GPR signature (ice-bedrock reflection) where visible, based on the amplitude of the signal. Where the signal is lost, e.g. due to high meltwater content, high ice thickness, or high bedrock slope, the picking is based on the suggestions from the three mathematical models. In the end, a second run of the GlaTE model assembles the estimations from the algorithm and the manually picked GPR measurements to provide a final ice-thickness map. The Rutor glacier, according to the methodology proposed, is estimated to cover an area of about 7.45 km^2 and store about 515 million m^3 of ice in 2021, compared to the previous estimate of 150 million m^3 made in 2008. The methodology is simple to reproduce and may simplify and ease future GPR surveys of temperate glaciers, especially when facing noisy data due to meltwater content or other reflectors such as debris. Another advantage is to directly produce an ice thickness map of the whole glacier, without relying on pure interpolation of sparse GPR data. The prior run of such models is also advised during the planning of glacier surveys, together with GPR forward modeling, to help choose the best GPR antenna frequency according to the expected ice thickness.

https://doi.org/10.5194/egusphere-2024-2569
Preprint. Discussion started: 25 September 2024

1 Introduction

Temperate valley glaciers are a characteristic feature of mountain chains in temperate zones, such as the European Alps, and have a pivotal role in the hydrological cycle (Milner et al., 2017). Studying the glacier processes and changes linked to the current climate crisis often requires a central task: a reliable estimate of their inner composition and geometry: bedrock topography, crevasses, cavities, debris, and meltwater (Haeberli et al., 2019). Such temperate glaciers are characterized by containing temperate (or "warm") ice at the temperature-pressure melting point. Indeed, colder ice zones often exist in temperate glaciers, but they are limited to specific areas or seasons, e.g. where the snow melts late in the warm season, or in the areas where the ice is thin and provides little isolation to the geothermal heat during the cold season (Suter et al., 2001; Reinardy et al., 2019). Widespread temperate conditions in a glacier mean that virtually every heat input, mainly by solar radiation from above or by geothermal heat from below, causes the production of meltwater.

A high meltwater content in glaciers may challenge the quality of geophysical surveys performed by Ground Penetrating Radar (GPR), one of the most used techniques for surveying ice masses (Colucci et al., 2015; Forte et al., 2015; Urbini et al., 2019). Since meltwater has very different electrical permittivity compared to ice, it reflects and scatters the electromagnetic wave, hindering the signal from traveling until the bedrock and being detected on its way back (Reinardy et al., 2019). Smaller-scale heterogeneities generate weak or undetectable responses but their presence has an impact on the signals as they pass by. The heterogeneities extract energy as the EM field passes and scatter it in all directions (Jol, 2009). This issue was widely studied by (Rutishauser et al., 2016), who analyzed a large dataset of GPR data acquired on the Swiss glaciers and stated that, according to each specific glacier, the bedrock interface could be detected only in 12-69% of the data. GPR signal scattering rarely occurs in arctic cold glaciers, but when it is detected in some areas, it may be evidence that temperate conditions and meltwater are the cause (Karušs et al., 2022). Another common source of noise in GPR sections is the presence of debris inside or covering some glaciers (Colombero et al., 2019), due to phenomena such as adfreezing and entrainment of sediments into the basal ice layer (Weertman, 1961). Also, air bubbles trapped in ice cause scattering of GPR signal, which analysis allows distinguishing different types of ice, such as firn and superimposed ice (Langley et al., 2009). The scattering problem has already been noticed in the study of the Rutor glacier, the third-largest glacier in Aosta Valley, Southern Europe Alps. The details about the Rutor glacier and the GPR interpretation problems raised in previous studies are reported in the Study site paragraph. Another issue of GPR surveys on glaciers is the resolution: since GPR antennas are carried on straight lines, often separated by hundreds of meters, they only investigate discrete parts of the glacier. For example, if no GPR section passes on the zone where the thickness is highest, one can not know which is the maximum glacier thickness. Resolution and speed of investigation have always been a compromise.

In this paper, the Rutor glacier is investigated with two new GPR datasets, acquired in May 2012 with a helicopter-based survey and in May 2022 with a ground-based survey. Analyzing these new datasets, it is clear the uncertainty and difficulty in detecting the radar reflections of the ice-bedrock interface, due to the high scattering of the signal in most parts of the glacier, probably caused by meltwater content. The scattering zone is often located at around 20 meters of depth, and may easily be misinterpreted as the ice-bedrock interface, possibly explaining the previous doubtful estimates of ice thickness.

https://doi.org/10.5194/egusphere-2024-2569
Preprint. Discussion started: 25 September 2024

To address this problem encountered on the Rutor glacier, but common to other temperate glaciers, ice-thickness modeling algorithms may help the analyst in the interpretation of scattered GPR sections. Those algorithms require, as input, the glacier surface topography, which can be retrieved for example by satellite imagery. Some algorithms have obtained much acknowledgment in recent years, see for example the ITMIX project (Farinotti et al., 2017) in which many ice-thickness algorithms are compared on the same set of glaciers. One of the conclusions of that research is that considering an average output from different models provides a more reliable ice-thickness estimate than finely tuning just one model.

The ice-thickness modeling algorithms employed in this work are three different models, the open source GlabTop2 (Frey et al., 2014), OGGM (Maussion et al., 2019) and GlaTE (Langhammer et al., 2019b). Thanks to a Digital Elevation Model (DEM) by drone photogrammetry survey performed in 2021 (Macelloni et al., 2022), the ice thickness is predicted using the three models. Topographic profiles corresponding to the GPR traces acquired in 2012 and 2022 are extracted. During the manual picking phase of the GPR data interpretation, the results from the three models are superimposed in the figure to help recognize the most probably correct ice-bedrock interface, often submerged by noise due to the meltwater content. Finally, a second run of the GlaTE model constraints the estimate of the ice thickness using the ice-bedrock interface pickings of the GPR data, providing a final model of the inner geometry of the glacier.

Overall, this methodology was confirmed to help avoid the erroneous picking of the first reflective interface, which could be interpreted as the ice-bedrock interface, but is probably due to meltwater content. The detection of the Rutor glacier geometry was eased and it should be more reliable compared to the previous estimate, even if the GPR data have a physical limit in detecting the bedrock interface and this fact challenges any certainty about the Rutor glacier bedrock topography. Also, in the areas where no GPR data is present, the ice thickness estimation is based on simplified physically-based equations, which can be considered more reliable than pure interpolation between GPR sections. The geometry model of the Rutor glacier updated at 2021 retrieved in this study may also be useful for ongoing studies about the hydrology and sediment transport of the area.

2 Study site

Located in the southwestern European Alps, the Rutor massif hosts the third-largest glacier in the Aosta Valley. The massif develops on multiple terraces, on which the Rutor glacier has advanced or retreated according to the climate variations, shaping the basin morphology (Vergnano et al., 2023). In the past, the Rutor basin was the theater of geomorphological events and processes, often related to glacial lake outburst floods, well documented since the second half of the 19^{th} century. After the Little Ice Age (LIA), which corresponded to a local maximum of the extent of the glaciers, the ice masses started to melt and shrink, drawing the attention of the scientific community. Consequently, many proglacial lakes have formed in place of previous glacier overdeepenings. The first historical document which extensively reviewed the Rutor basin, and also collected all the available previous literature, was written by Baretti (1880). Thanks to scientists of the 19^{th} century and the beginning of the 20^{th} century, the Rutor basin was deeply investigated from different points of view (e.g. biology, engineering, geology) (Baretti, 1880; Favre, 1867; Sacco, 1917; Monti, 1906; Carrel, 1867; Preller, 1918). The study of the Rutor glacier has continued after the literature of the beginning of 1900 and was driven by the interest of different disciplines and perspectives (Villa et al.,

https://doi.org/10.5194/egusphere-2024-2569
Preprint. Discussion started: 25 September 2024

2007; Macelloni et al., 2022; Armando and Charrier, 1985; Burga, 1991; Orombelli, 2005; Villa et al., 2008; Strigaro et al., 2016; Viani et al., 2016; Badino et al., 2018). Among others, the Glacier Lab research group from Politecnico di Torino is currently studying the Rutor basin from a multiisciplinary perspective (Corte et al., 2024; Gizzi et al., 2022; Vergnano et al., 2023) Nowadays, the Rutor glacier is 7.5 km^2 wide and it is situated in the municipality of La Thuile. It has retreated, since the beginning of 1900, to an upper terrace, allowing the formation of new proglacial lakes near each of its three tongues (western, central, and eastern). Its tongues are situated on the northern side of the glacier at about 2550 m a.s.l. (the eastern tongue) and 2650 m (the central and the western tongue). Its highest elevation is about 3440 m, near the southern outline.

In the recent decades, the glacier experienced a significant retreat, linked to the acceleration of climate warming. The ice thickness lost from 2008 to 2021 was computed by the difference between two Digital Elevation Models (DEMs) and displayed in Figure 1. Previous GPR surveys (1996-2006) reported an average thickness of the glacier of 17.5 m (a volume of 150 million m^3 divided by an area of 8.5 km^2) (Villa et al., 2008, 2007). However, probably this estimate could be far from the actual value, because the changes in the glacier surface topography observed from 2008 to 2021 evidenced a loss of more than 20 vertical meters of ice in about 1/4 of the current glacier area (especially in the tongue area, as in Figure 1) for a total ice volume loss of about 100 million m^3. Moreover, many examples of other alpine glaciers with a similar extension consistently show greater ice thickness (Grab et al., 2021). The analysis performed by Viani et al. (2020) expresses similar considerations about the difficulty of interpreting the correct bedrock geometry of the Rutor glacier.

3 Methods

The methodology tested in this paper to overcome the difficulties in interpreting the GPR data of the Rutor glacier consisted of the following steps:

1. To collect and analyze new and updated GPR datasets from two acquisitions, a helicopter-based survey made in 2012 and a ground-based survey made in 2022. In Figure 2, the location of the GPR sections is drawn.
2. To run three algorithms (GlabTop2, GlaTE, OGGM), which, based on the surface topography, estimate the ice thickness. This step is shown in Figure 4.
3. To extract the ice thickness estimated by the models in the same locations of the GPR paths, thanks to the v.sample tool of QGIS, GRASS plugin (QGIS-Development-Team, 2024), using a bilinear interpolation method, as in Figure 5.
4. To perform the manual picking of the reflection events in the GPR data with the help of the estimations from the three models, to limit the uncertainties in detecting the correct ice-bedrock interface.
5. To run for a second time the GlaTE algorithm, constraining the estimations based on the surface topography with the GPR data.
6. To draw the final result: a map of the glacier ice thickness (Figure 6).

https://doi.org/10.5194/egusphere-2024-2569
Preprint. Discussion started: 25 September 2024

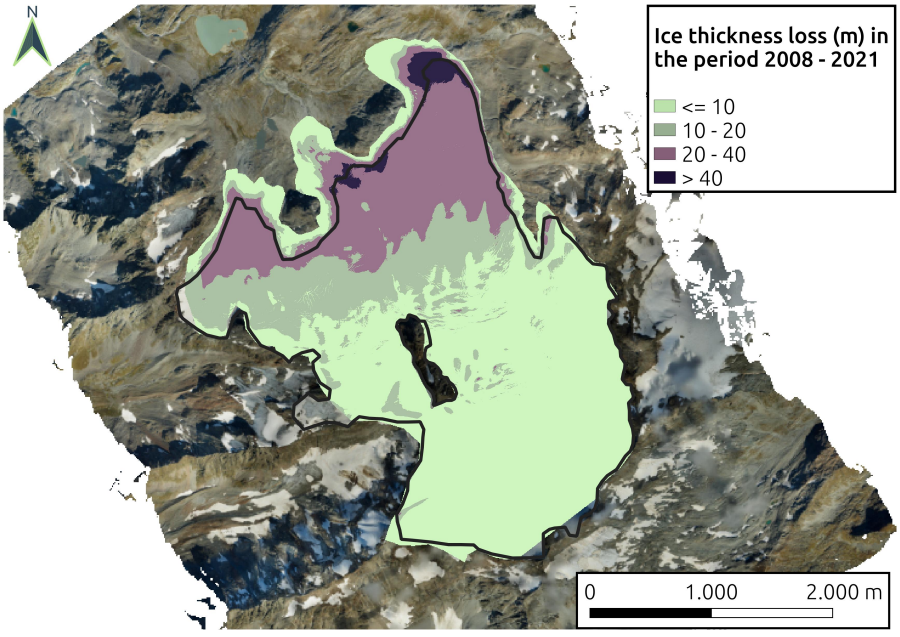

Figure 1. The Rutor glacier divided in four areas, according to how many meters it has subsided in the past decade (from 2008 to 2021). The black glacier outline is that of 2021. The colored glacier outline is taken from that of 2003, and this choice is visible in the light green areas near the three tongues of the glacier, which obviously did not change in altitude from 2008 to 2021 ("tokyo" color scale, according to (Crameri, 2021)).

Some topographical adjustments were needed in order to deal with GPR data from 2012 and 2022, the DEM of the glacier surface from 2021 used for GlaTE and GlabTop2 algorithms, and the DEM of the glacier surface from 2000 used in the OGGM algorithm. In other words, the GlaTE and GlabTop2 models depict the situation in 2021, OGGM in 2000, and GPR data in 2012. First, all data were reprojected into the same Coordinate Reference System (ED50, UTM 32 N), using the warp/reproject tool of QGIS software. With the same tool, using a bilinear-based triangulation method, the DEMs were undersampled to 20-m resolution, for computation time optimization and considered adequate to avoid artifacts generated by a too-fine resolution, according to GlaTE algorithm authors [Melchior Grab and Hansruedi Maurer, personal communication]. The DEM used for the OGGM algorithm, being 50-m resolution, was not undersampled.

To compare the three ice-thickness models generated by the three algorithms with the GPR sections of the 2012 survey, every model had to be "converted" to 2012, that is, the ice lost from 2000 to 2012 (in the case of OGGM) and from 2012 to 2021 (in case of GlaTE and GlabTop2), had to be considered in the comparison. For GlaTE and Glabtop2, since a good 2008 DEM of the glacier surface was available from the regional cartography (https://mappe.regione.vda.it/pub/geonavitg/geodownload.asp?carta=DTM99, last accessed: 13 October 2023), the ice lost from 2012 to 2021 was estimated by a simple linear interpolation between the 2008 glacier surface elevation and the 2021 glacier surface elevation, supposing that the glacier melting in those years was constant on average. The ice lost from 2012 to 2021 was added to the GlaTE and GlabTop2 thicknesses, to allow comparing

https://doi.org/10.5194/egusphere-2024-2569
Preprint. Discussion started: 25 September 2024

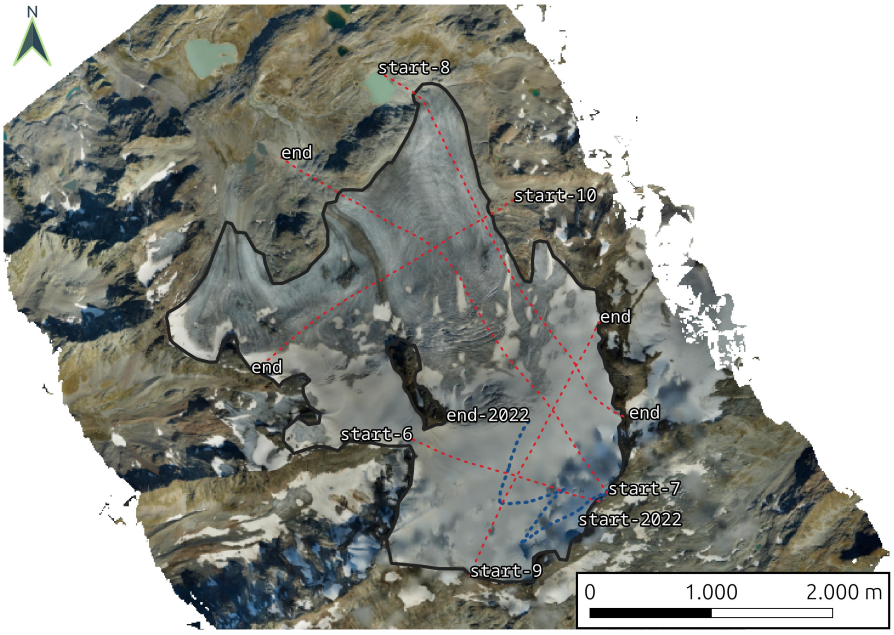

Figure 2. The GPR profiles of the Rutor glacier survey. Numbers from 6 to 10 and red dashed lines indicate the profiles of 2012, while blue dashed lines indicate the 2022 survey.

them to the 2012 GPR sections. An analogous procedure was applied to correct the 2000 thickness model produced by OGGM, to account for the ice lost from 2000 to 2012. For comparing the 2022 GPR profile to the models, no correction was performed for GlaTE and GlabTop2 2021 models, since the ice lost from 2021 to 2022 is negligible for the kind of comparison performed. After these corrections, the comparison between models and GPR could be done, as in Figure 5.

After the manual picking of the reflection events in the GPR data, the final GlaTE model, constrained by GPR data, was built. To achieve this, the GPR pickings, based on the 2012 survey, were corrected to 2021, by subtracting the ice lost from 2012 to 2021 from the thickness.

3.1 Ground-penetrating radar (GPR)

Low-frequency antennas were employed to survey the thick ice layers of the Rutor glacier. In the 2012 helicopter-based dataset, a GSSI single-frequency antenna with a central frequency of 70 MHz was employed. In the 2022 ground-based survey, a 40 MHz antenna, RIS ONE model with single-frequency antenna configuration, manufactured by IDS, was carried on ski by an operator. For both surveys, a constant acquisition speed was not always possible, therefore, in the processing steps, it was decided to display 1 trace per meter. The raw data were processed according to the following steps, using the commercial ReflexW software (Sandmeier, 2012), then visualized and compared with the results of the algorithms using the RGPR open source software (Huber and Hans, 2018).

https://doi.org/10.5194/egusphere-2024-2569
Preprint. Discussion started: 25 September 2024

1. Application of a band pass butterworth filter - from 55 to 80 MHz, to eliminate low frequencies and high frequencies, and a frequency spike around 90 MHz probably due to instrumental noise or helicopter interference.
2. Application of correct max. phase + move startime: a series of two processing steps suggested by Reflexw to perform an automatic time-zero correction.
3. Application of a background removal filter (x-direction average-trace removal over the entire profiles), to eliminate instrument noise constant in the x-direction.
4. Application of a make equidistant traces filter, to plot 1 trace per meter, especially important for the 2012 survey, since the helicopter was not flying constantly at the same speed.
5. Application of a gain filter called Energy decay: a gain curve in y-(time-) direction applied on the complete profile based on a mean amplitude decay curve, which is automatically determined (Sandmeier, 2012), to compensate the time-direction attenuation and geometric spreading of the signal.
6. Conversion of the y-axis from time to depth, assuming a constant velocity of the electromagnetic signal in the ice of 0.167 m/ns (Bohleber et al., 2017).
7. Manual picking of the ice-bedrock interface with the guidance of model estimations.

The data were not migrated. Some attempts with simplified velocity models were tried, without any significant enhancement.

3.2 Ice thickness modeling algorithms

Despite being recent, the three ice-thickness modeling algorithms chosen, GlabTop2, GlaTE, and OGGM, have quickly gained success among researchers. According to the Scopus database considering the publications until February 2023, at least 10 articles used GlaTE, more than 50 used GlabTop2, and about 200 employed OGGM. Those numbers can be explained by the fact that OGGM is a framework of models that can be employed for wider objectives, and not only for the ice thickness estimation, as GlaTE and GlabTop2. OGGM was first developed in 2016, GlabTop2 in 2014, and GlaTE is the most recent, published in 2019.

All the algorithms used in this study require as input a digital elevation model (DEM) of the glacier surface, and they perform algorithms based on theoretical considerations of ice flux mechanics. In this study, they were employed for two objectives. First, to provide a first estimate of the ice thickness distribution of the Rutor glacier, in order to drive the detection of the interface during the manual picking of the GPR sections. Second, the GlaTE model (introduced later in this paragraph) was employed to provide a final estimation of the Rutor glacier ice thickness, based on both model estimations and GPR data constraints.

The modeling algorithms required also some input parameters to run. They were checked for consistency with the physical problem object of study, but unless otherwise specified in the following, they were not changed from the default values, which were used in the studies, on similar alpine glaciers, performed by the writers of the algorithms. In the following, a brief explanation of the three algorithms is provided.

https://doi.org/10.5194/egusphere-2024-2569
Preprint. Discussion started: 25 September 2024

3.2.1 GlabTop2

The GlabTop2 (Glacier bed Topography 2) model assesses the distribution of ice thickness in a glacier starting from a DEM file and a mask file containing the outline of the glacier (Frey et al., 2014). It employs an algorithm first developed by (Linsbauer et al., 2012), but slightly modified to avoid the computation of the glacier flow lines:

$$h_f = \frac{\tau}{f \cdot \rho \cdot g \cdot sin(\alpha)} \tag{1}$$

where h_f is the mean ice thickness along the central glacier flow line, f is a shape factor, τ the shear stress at the glacier base, calculated with an empirical formula based on the elevation range of the glacier ΔH (equation 2), and expressed in kPa, ρ the ice density ($910\ \mathrm{kg/m^3}$) (Langhammer et al., 2019a), g is the gravity acceleration, and α is the surface topography slope.

$$\tau = 0.5 + 159.81\Delta H - 43.5\Delta H^2 \tag{2}$$

The first processing step employed by the algorithm is an initial approximation of ice thickness in some random cells of the domain, based on the surface slope of a sufficiently large buffer zone around the cell. Then, the ice thickness of the remaining cells is estimated with a simple inverse distance weighting algorithm. The two steps are repeated for n times and the results are averaged.

Further details are provided in the appendix of Frey et al. (2014). The code is open source and runs in Python; at the time of writing, the code is available at https://github.com/WilcoTerink/GlabTop2-py.

3.2.2 GlaTE

GlaTE (Glacier Thickness Estimation) is also based on equation 1, but with a different estimation of the shear stress τ and a different implementation algorithm, according to the work of Clarke et al., 2013 (Clarke et al., 2013). In this work, it was employed in two separate steps: first, to provide an initial estimate of the glacier thickness, together with the other two models, and secondly, to calculate a final estimate of the ice thickness with GPR data constraining the model. In fact, the strength of GlaTE is the integration between the estimation model (based on surface DEM and glacier outline like GlabTop2) and ground-proof data such as GPR profiles. GlaTE performs an inversion procedure, constraining the ice thickness results such that they match, with a certain degree of uncertainty, a series of GPR data, such that they follow some smoothness requirements, respect the glacier perimeter, and the values at the border of the glacier are consistent with the average terrain slope outside the glacier. The system of equations to be inverted can be summarized into the matrix in equation 3 :

$$\begin{bmatrix} \lambda_1 G \\ \lambda_2 L \\ \lambda_2 B_{gb} \\ \lambda_3 B_0 \\ \lambda_4 S \end{bmatrix} h_{est} = \begin{bmatrix} \lambda_1 h_{GPR} \\ \lambda_2 \nabla h_{Clarke} \\ \lambda_2 \nabla h_{boundary} \\ \lambda_3 \\ \lambda_4 \end{bmatrix} \tag{3}$$

https://doi.org/10.5194/egusphere-2024-2569
Preprint. Discussion started: 25 September 2024

where h_{GPR} is the ground proof GPR data, h_{Clarke} is the ice thickness modeled according to Clarke's algorithm, ∇h_{bound} is the gradient of terrain slope at the outside boundary of the glacier. The operator G ensures the constraint with GPR data, L with the ice thickness modeled according to Clarke's algorithm, B_{gb} with the gradient of outside terrain slope, B_0 with the 0 thickness at the boundary, while S is a smoothing constraint. The λ factors are weighting factors and are varied in an iterative manner, in order to give maximum weight to the Clarke model and the smoothness constraint while fitting the GPR data (Grab et al., 2021). The ice density was estimated at 910 $\mathrm{kg/m^3}$. The creep factor (or ice softness) A was estimated to be about $2.4 \cdot 10^{-24}\ \mathrm{s^{-1}Pa^{-3}}$, neglecting its temperature dependence as if the glacier was at 0°C (Cuffey, 2002), since the Rutor glacier shows temperate conditions (even if this could not be true for the entire glacier) (Cook et al., 2020). The exponent of Glen's flow law was fixed at 3, as considered the best approximation in the absence of data about the ice fabric (Glen and Paren, 1975). Eventual debris presence, which can be added to the algorithm, was not taken into consideration, because from the orthophotos, and by visual investigation, there is no evident thick debris cover in the ablation area of Rutor glacier. For further details, see Langhammer et al. (2019b); Grab et al. (2021); Schwanghart and Scherler (2014).

The model is open source, it runs in MATLAB environment and at the time of writing it is available at https://gitlab.com/hmaurer/glate.

3.2.3 OGGM

The OGGM (Open Global Glacier Model) is an open-source collection of algorithms written in Python that provides different insights about glaciers, for example, thickness, runoff meltwater, and future predictions based on climate variations. In this work, only the OGGM bed topography inversion algorithm was employed, which is based on the work of (Farinotti et al., 2009). The main flux equation OGGM is based on is equation 4

$$q = uS = \left(f_d h \tau^n + f_s \frac{\tau^n}{h} \right) S \tag{4}$$

where h is the ice thickness, q is the ice volume flux, u is the ice flow velocity, S is the section, which in case of a simplified parabolic section is $= 2/3 \cdot h \cdot width$, n is the exponent according to Glen's law (=3), τ is the shear stress, f_d is proportional to the ice softness A ($f_d = 2A/n + 2$), f_s is a sliding factor, neglected for simplicity in this run of the algorithm. The flux q in a section is also equal to the mass balance (mass input - output due to precipitations and melting) integrated over the area of the glacier situated above the section considered, under the simple assumption of equilibrium, which is unfortunately not exactly true, given the rapid changes in the volume of glaciers due to the climate crisis. During the inversion process, one parameter, the ice softness A, is allowed to vary, in general about one order of magnitude, from the standard value of $2.4 \cdot 10^{-24}\ \mathrm{s^{-1}Pa^{-3}}$.

Further details and the implementation in the OGGM framework are described in (Maussion et al., 2019) and the software is freely available at https://www.oggm.org.

The model was run based on a DEM from 2000 (JPL, 2020), then the ice thickness result was corrected to 2021 by subtracting the ice lost from 2000 to 2021 (based on DEM subtraction pixel by pixel). Even if this fact can surely introduce uncertainties, it is also a challenging test of such algorithms, i. e. to see if their results can be reasonably compared even if they start from different DEMs.

https://doi.org/10.5194/egusphere-2024-2569
Preprint. Discussion started: 25 September 2024

4 Results

The graphs pictured in this section, which follow the steps of the proposed methodology are the following:

1. An example of a processed GPR section on the temperate Rutor Glacier showing the difficulties in its interpretation, due to scattering and random noise (Figure 3).
2. The ice thickness maps produced by the three models (GlabTop2, GlaTE, and OGGM) without GPR data constrain (Figure 4).
3. An example ice-thickness profile extracted from the previous models, matching the location of a GPR section, used as a base to pick more easily the reflections of the ice-bedrock interface (Figure 5). The other GPR sections are shown in the Appendix.
4. The final ice-thickness map produced by the GlaTE model constrained by the GPR data, which were analyzed as the previous point (Figure 6).

The first result shown here is an example section of the heli-based 2012 dataset, section number 7 (Figure 3, location of the section shown in Figure 6).

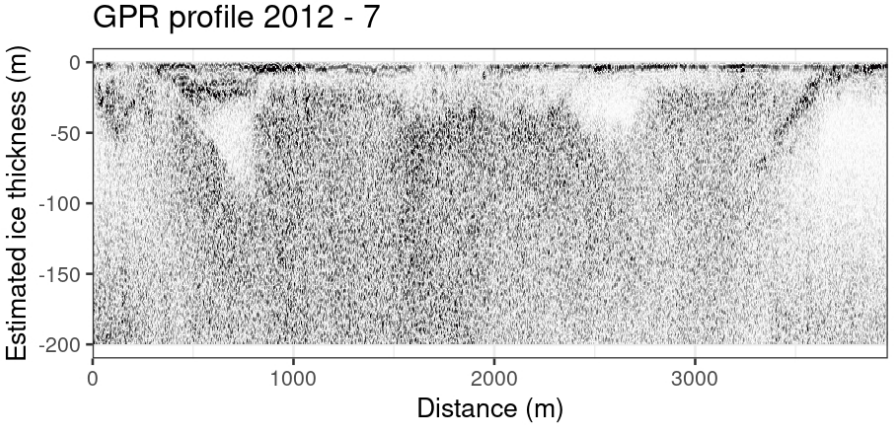

Figure 3. The GPR section number 7 of the heli-based 2012 dataset. The thickness scale was built assuming a constant velocity of the electromagnetic signal in ice of 0.167 m/ns. The white area is compact firn or ice without water. The ice-bedrock interface is well visible only on the right part of the image.

Looking at the central part of Figure 3, one could be tempted to interpret the area without reflections, pictured in white, as ice, and the first black reflection zone as the bedrock. However, on the right side of the plot, the clearly submerging ice-bedrock interface shows that the former is probably not the correct interpretation. Elsewhere, possible ice-bedrock interfaces may be spotted and somewhat followed in the GPR section, but the interpretation is far from straightforward. This clutter phenomenon

https://doi.org/10.5194/egusphere-2024-2569
Preprint. Discussion started: 25 September 2024

has been previously reviewed by Rutishauser et al. (2016). This is not an ideal situation to draw a thickness map of the glacier, and some other reasoning is needed to tackle, or at least estimate, the data uncertainty. It is argued that a similar interpretation problem could have arisen in the 2008 dataset analyzed by (Villa et al., 2008), and this could explain the unexpectedly shallow thickness calculated there.

In Figure 4 the three ice-thickness maps, respectively produced by GlabTop2, GlaTE, and OGGM models without GPR constraints are shown.

The three raster maps in Figure 4, although produced with different models, show a very similar reconstruction of the glacier geometry. The total ice mass estimated by the models, in millions m^3, is: OGGM = 510, GlaTE = 520, GlabTop2 = 580. Their thickness value was bilinearly interpolated at the points corresponding to the GPR survey paths, to produce comparison plots such as Figure 5. All the other GPR sections with the model estimations are shown in detail in the Appendix.

All the GPR sections from the 2012 and 2022 surveys were analyzed taking into consideration the estimations provided by the three models. In such a way, a probably more correct picking of the ice-bedrock interface was performed. Lastly, all the pickings were gathered in a dataset as input of the GlaTE model to produce the best estimate possible of the ice thickness distribution of the Rutor Glacier in 2021, shown in Figure 6 (total ice mass = 515 million m^3).

https://doi.org/10.5194/egusphere-2024-2569
Preprint. Discussion started: 25 September 2024

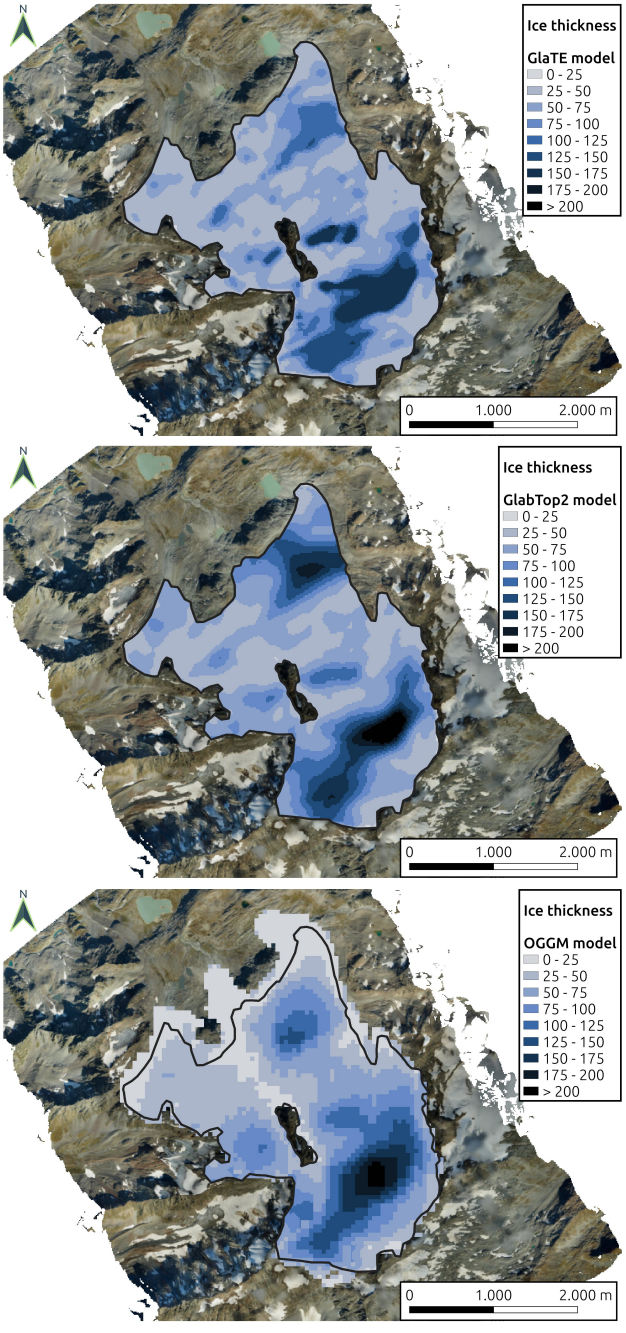

Figure 4. Ice thickness maps of the Rutor glacier produced with GlaTE, GlabTop2, and OGGM models without any constrain by ground-proof data, but only with topographic surface data as input ("oslo" color scale, according to (Crameri, 2021)).

https://doi.org/10.5194/egusphere-2024-2569
Preprint. Discussion started: 25 September 2024

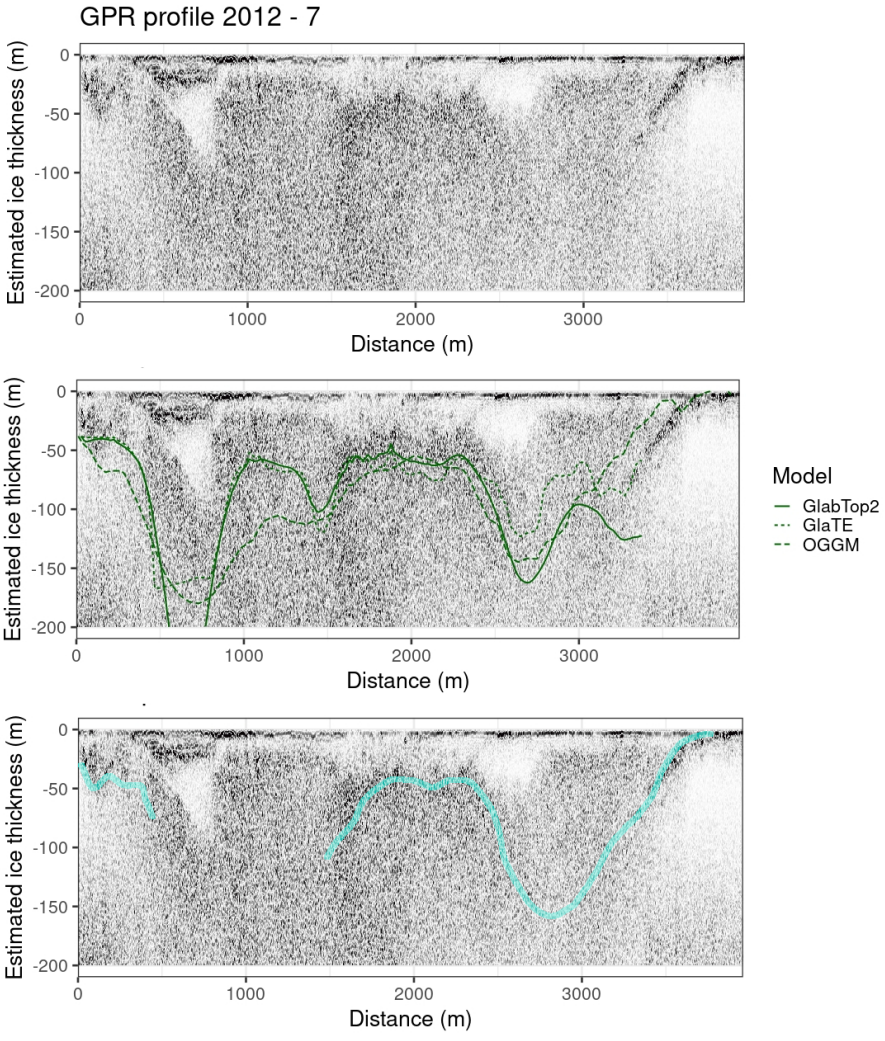

Figure 5. An example GPR section with the estimation from the three models overlayed: long dash line, OGGM, continuous line, GlabTop2, short dash line, GlaTE. The manual picking which was possible by comparing the GPR profiles and the models is displayed in light blue.

https://doi.org/10.5194/egusphere-2024-2569
Preprint. Discussion started: 25 September 2024

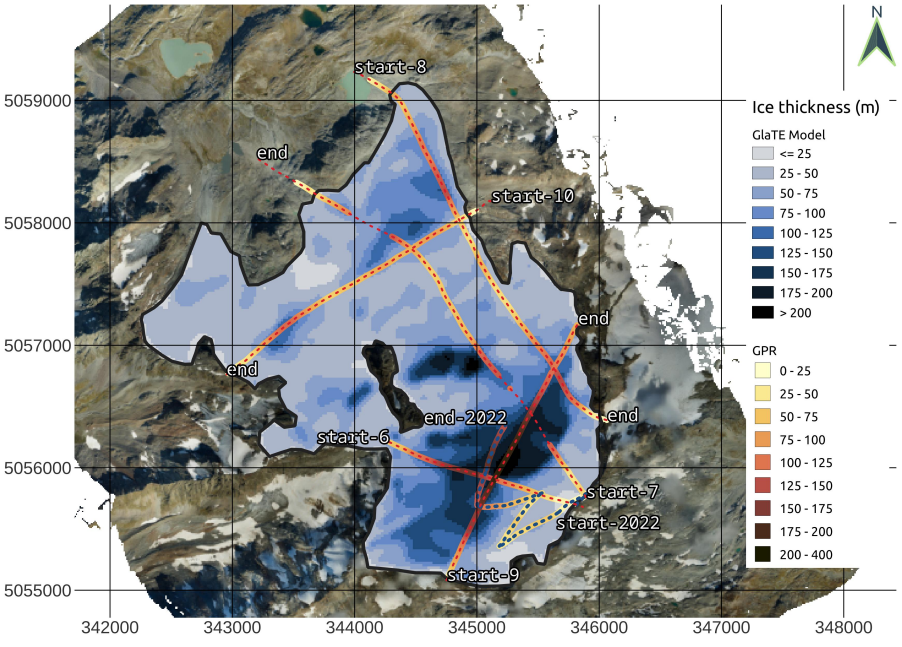

Figure 6. The final model of the Rutor glacier ice thickness obtained by GlaTE model constrained with the GPR data ("oslo" color scale, according to (Crameri, 2021)). The ice thickness of GPR data is plotted in a different color scale ("lajolla", according to (Crameri, 2021)), to show that in the crossings between different GPR sections, the picked thickness is fairly similar.

https://doi.org/10.5194/egusphere-2024-2569
Preprint. Discussion started: 25 September 2024

5 Discussion

5.1 Comparison of the three ice-thickness modeling algorithms

The three different algorithms, in their first run without GPR constraints, gave fairly similar estimates of ice thickness (in millions m^3, OGGM = 510; GlaTE = 520, GlabTop2 = 580). The resolution of GlaTE and GlabTop2 models was set at 20 m, even if the input data could allow a much finer resolution. This strategy was employed because a finer resolution might lead to misleading structures in the resulting bedrock topography (Melchior Grab, personal communication) and for following a principle of simplicity (Sober, 2015). The OGGM model was tested with a different input DEM, from 2000 (JPL, 2020), with 50 m resolution, and then the estimated ice thickness was then corrected with the ice-thickness loss between 2000 and 2021, by subtracting the two DEMs. The OGGM estimations were qualitatively similar to those of GlaTE and GlabTop2, except in some minor parts, notwithstanding their differences in the algorithms employed and in the input data. The consistency between different algorithms shows their overall reliability. This observation is consistent with a previous review (Farinotti et al., 2017), which stated that algorithms based on surface topography can provide fairly accurate estimations of ice thickness. They can provide gross estimates of ice volume or future position of lakes in place of glacier overdeepenings (Viani et al., 2016), with a lower effort in terms of input data and computational time compared to a GPR survey. However, the performance of the algorithms was poor near the outline of the glacier: here, the thickness was generally overestimated.

5.2 Joint interpretation of GPR and ice-thickness algorithms

GPR and ice-thickness algorithms were interpreted together in all the GPR sections of the Rutor glacier, which were both helicopter- and ground-based. The various GPR sections had a different degree of readability. In some of them, the ice-bedrock interface could be followed relatively easily, such as for section 2012 - 8 (Figure A3). In that case, the three algorithms (GlaTE, GlabTop2, OGGM) were generally consistent with the ice-bedrock interface depicted by the GPR reflections, demonstrating the overall good quality of the retrieved ice-thickness models, already proven by Farinotti et al. (2017). In most other sections the bedrock was rapidly lost below about 50 m of depth. In general, the signal suffered from scattering, due to the many reflection events distributed throughout the glacier, except some areas near the outline. This phenomenon made the interpretation of these sections challenging. In this sense, the ice-thickness modeling algorithms were fundamental to retrieve the bedrock topography where it could not be detected by the GPR and to avoid misinterpretations; more confidence was given where the models were strictly consistent with each other. No particular improvement was seen when using a ground-based 40 MHz GPR antenna compared to the heli-based 70 MHz antenna. Specific comments on the interpretation of each GPR section are available in the Appendix section.

This joint interpretation avoided the mistake of interpreting the first layer without reflections (white in the GPR sections) as ice, and the first reflective zone (scattered black) as bedrock. The deepening reflection in the right part of Figure 3 shows clearly that the ice-bedrock interface is not related to the scattered reflective zone seen in all the GPR sections at 20-40 m depth. Therefore, manually picking the ice-bedrock interface on GPR sections only after seeing what was the estimate from

https://doi.org/10.5194/egusphere-2024-2569
Preprint. Discussion started: 25 September 2024

the algorithms was very helpful in this context. In particular, the algorithms were useful below about 50 m depth, where the GPR signal was too attenuated.

The ice thickness estimated with the second run of the GlaTE model constrained by GPR data is about 515 million m^3, which is not far from the estimates without GPR data. This result may be overall affected by the fact that the picking of the GPR sections was indeed guided by the model estimations, but since GPR and models were fairly consistent to each other in the most clear sections (such as 2012 - 8, Figure A3), this is not considered a significant bias. This estimate is more than three times larger than that previously calculated (150 million m^3, (Villa et al., 2008)). This is considered to be a better estimate compared to the previous one, due to the matching between GPR and ice-thickness models, and the good reputability of ice-thickness models of such kind, as proven in the ITMIX project (Farinotti et al., 2017).

5.3 Advantages and limitations of the methodology

Without the help of ice-thickness models, only about 20% of the GPR lines clearly identified the bedrock (3.3 km out of 17 km). This is a low value, but comparable to the complete review on this issue performed by Rutishauser et al. (2016), which observed that, depending on the glacier, only from 12 to 69 % of the bedrock could be identified. This review was performed on Swiss glaciers, which have climatic conditions similar to the Rutor glacier. Moreover, better results were achieved only in alpine glaciers where cold conditions are more widespread. Therefore, this methodology could represent a tool to increase the "pickable" regions of scattered GPR sections. The zones more difficult to interpret are, according to (Rutishauser et al., 2016): where the ice is thickest, where the bedrock slope is highest, and where there is meltwater. In the dataset analyzed here, the higher ice thickness is recognized to be a cause of lower clearness of GPR sections, and meltwater content is highly probable, given the scattered GPR sections and the relatively warm climate in which the Rutor glacier is situated.

The integration of the two methods seems the most viable option to provide a more reliable estimate of ice thickness than one method alone, especially in the absence of costly boreholes intercepting the bedrock at depth. This is a great achievement, because those algorithms are open-source and require low effort to use, and their reliability and comparability with GPR data has been observed in this and previous research. They also can complement the design of a GPR survey to select the best antenna frequency, based on the expected ice depth, alongside forward modeling to produce synthetic data.

However, many drawbacks have to be considered. First, the difficulties in interpreting the GPR data, which represent the most significant source of possible errors and subjectivity; then, inaccuracies in the estimates provided by the different models, which are a simplification of the real system, and rely on estimates of many parameters; also, possible errors in the glacier perimeter, which is an important input of the algorithms, due to the manual observation of the aerial orthophoto (Santin et al., 2023). Moreover, the fact that the topographic surveys to obtain the DEMs had different resolutions and happened at different years, and the GPR surveys also were carried out during other years, required a time interpolation of the ice thickness, to take into account the progressive melting of ice, which introduced another deviation from the real value of ice thickness. However, the algorithms produced reasonably comparable models even from starting from different DEMs, therefore this can be seen as a point of strength of the methodology. The combination of multiple methods was then key to giving more reliability to the proposed methodology and miimizing the error effects; however, after an overall consideration of every possible source of

https://doi.org/10.5194/egusphere-2024-2569
Preprint. Discussion started: 25 September 2024

error, a deviation of at least + - 100 million m^3 of ice should be considered, which corresponds to an average ice thickness of about + - 13 meters.

5.4 Future applications and perspectives

The GPR alone, while not performing always well on temperate glaciers, remains a very good instrument to investigate ice masses, even in temperate conditions. Aside the bedrock geometry detection, two examples of applications of GPR on glaciers that could increase in importance due to climate warming are the investigation of cavities and the distinction between cold and warm ice zones inside a glacier. The latter, according to Reinardy et al. (2019) and Comiti et al. (2019), plays an important role in regulating the sediment transport at the glacier base, and can be retrieved from the distribution of reflections (due to meltwater) in the GPR sections: it could be explored in the future also on the Rutor glacier itself, potentially reusing the dataset analyzed here.

This dataset is openly released and available for further studies. It can be used for comparisons or regional assessments of the meltwater content in temperate Alpine glaciers. It will also be helpful for ongoing studies on the water mass balance and sediment transport of the Rutor basin. Since the Rutor basin hosts many proglacial lakes, the map reveals the possible position of future lakes, in place of the overdeepenings of the bedrock topography (Figure 6). Their location is consistent with what was estimated by a previous work (Viani et al., 2020). The shrinking of Rutor glacier is speculated to occur mostly in the following decades, given its volume of 515 million m^3 and its loss of 100 million m^3 from just 2008 to 2021. After a few decades, little ice is expected to be still contained in the Rutor glacier.

To summarize, if one has the possibility to carry out a geophysical survey, the ice-thickness modeling algorithms in combination with the GPR are the most effort-effective way to represent, with a certain degree of uncertainty, a glacier bedrock geometry. This is in line with the philosophy behind the GlaTE algorithm, built to constrain a topographical-data-based algorithm with "ground-proof" GPR data.

6 Conclusions

Investigating glacier substructures with GPR may be challenging in temperate glaciers, where the widespread water content and debris cause signal scattering, making it difficult to distinguish the ice-bedrock interface. The Rutor glacier had already been surveyed with GPR in the past but, due to these interpretation difficulties, was estimated to have a very small ice thickness, of about 17.5 m. This estimation proved to be wrong after observing that, in the 2010-2020 decade, the Rutor glacier lost more than 20 vertical meters in 1/4 of its area, while reducing its extension only by a fraction.

The analysis of two new GPR datasets from 2012 (helicopter-based) and 2022 (ground-based) confirmed the difficulty in reliably detecting the ice-bedrock interface. Therefore, the open-source GlabTop2, GlaTE, and OGGM ice-modeling algorithms were tested, to understand how they could support the interpretation of difficult datasets acquired on temperate glaciers. First, those algorithms were run with only the glacier surface topography as input. Then, their estimated thickness was overlapped to the GPR sections, providing a substantial help in manually picking the ice-bedrock interface. In particular, this methodol-

https://doi.org/10.5194/egusphere-2024-2569
Preprint. Discussion started: 25 September 2024

ogy avoided misinterpreting meltwater-rich areas as the ice-bedrock interface. Finally, a second run of the GlaTE algorithm produced an ice-thickness model of the Rutor glacier constrained by GPR data.

A prior run of two or three ice-thickness modeling algorithms, such as the ones tested in this study, is advised before analyzing GPR data on a glacier. Moreover, they can help to design the survey together with GPR forward modeling: for example, one can choose a lower frequency antenna if some thick ice areas are expected. The ice-thickness map produced and the dataset presented can also be reused for future local studies on the Rutor basin.

Code and data availability. The ice thickness map of the Rutor glacier in 2021 produced in this work is available in the supplementary materials.

The 2012 GPR dataset is available on a Zenodo repository at: https://doi.org/10.5281/zenodo.8027417

The 2021 DEM used for the GlaTE and GlabTop2 algorithms, together with the ortophoto used to draw the glacier outline, is available on a Zenodo repository at: https://doi.org/10.5281/zenodo.7713299

The 2000 DEM used for the OGGM algorithm is available at: https://doi.org/10.5067/MEASURES/NASADEM/NASADEM_HGT.001

The three ice-thickness modeling algorithms are available respectively at:

OGGM: https://oggm.org/

GlaTE: https://gitlab.com/hmaurer/glate

GlabTop2: https://glabtop2-py.readthedocs.io/en/latest/index.html

Author contributions. Conceptualization: A.V.; Data Curation: A.V.; Formal Analysis: A.V.; Funding Acquisition: A.G. and D.F.; Investigation: D.F.; Methodology: A.V., A.G. and D.F.; Project Administration: A.G.; Resources: A.G. and D.F.; Software: A.V; Supervision: A.G.; Validation: A.V.; Visualization: A.V; Writing: A.V..

Competing interests. The authors declare no competing interests are present

Acknowledgements. Thanks to Umberto Morra di Cella and the regional environmental protection agency of Aosta Valley, Italy (ARPA Val d'Aosta) for the 2012 dataset. Thanks to Fabio Villa for his help in understanding the Rutor glacier GPR and topography datasets. Thanks to Maurizio Ercoli, Emanuele Forte, Michele Freppaz and Chiara Colombero for their precious suggestions on the manuscript. Thanks to Myrta Maria Macelloni, Isabella Pisoni, Elisabetta Corte, and Alberto Cina for their help with the topographical data and for the 2021 Digital Elevation Model. Thanks to Hansruedi Maurer and Melchior Grab for their help about the GlaTE modeling algorithm. Thanks to Emanuel Huber for his support about the RGPR open source software. Thanks to LeldeBry, mainainer of GlabTop2 Github repository, for his help with software.

https://doi.org/10.5194/egusphere-2024-2569
Preprint. Discussion started: 25 September 2024

References

Armando, E. and Charrier, G.: The peat formation of the Rutor Glacier (Aosta Valley). Results obtained by palynostratigraphic study of new peat outcrops near the glacier snout, Geografia Fisica e Dinamica Quaternaria, 8, 144–149, 1985.

Badino, F., Ravazzi, C., Vallè, F., Pini, R., Aceti, A., Brunetti, M., Champvillair, E., Maggi, V., Maspero, F., Perego, R., and Orombelli, G.: 8800 years of high-altitude vegetation and climate history at the Rutor Glacier forefield, Italian Alps. Evidence of middle Holocene timberline rise and glacier contraction, Quaternary Science Reviews, 185, 41–68, https://doi.org/10.1016/j.quascirev.2018.01.022, 2018.

Baretti, M.: Il Lago del Rutor (Alpi Graje settentrionali), 14, 43–98, https://tecadigitale.cai.it/periodici/PDF/Bollettino/, 1880.

Bohleber, P., Sold, L., Hardy, D. R., Schwikowski, M., Klenk, P., Fischer, A., Sirguey, P., Cullen, N. J., Potocki, M., Hoffmann, H., and Mayewski, P.: Ground-penetrating radar reveals ice thickness and undisturbed englacial layers at Kilimanjaro's Northern Ice Field, The Cryosphere, 11, 469–482, https://doi.org/10.5194/tc-11-469-2017, 2017.

Burga, C. A.: Vegetation History and Palaeoclimatology of the Middle Holocene: Pollen Analysis of Alpine Peat Bog Sediments, Covered Formerly by the Rutor Glacier, 2510 m (Aosta Valley, Italy), Global Ecology and Biogeography Letters, 1, 143, https://doi.org/10.2307/2997428, 1991.

Carrel, G.: Le Lac du Rutor, 2, 400–403, https://tecadigitale.cai.it/periodici/PDF/Bollettino/, 1867.

Clarke, G. K. C., Anslow, F. S., Jarosch, A. H., Radić, V., Menounos, B., Bolch, T., and Berthier, E.: Ice Volume and Subglacial Topography for Western Canadian Glaciers from Mass Balance Fields, Thinning Rates, and a Bed Stress Model, Journal of Climate, 26, 4282–4303, https://doi.org/10.1175/JCLI-D-12-00513.1, 2013.

Colombero, C., Comina, C., De Toma, E., Franco, D., and Godio, A.: Ice Thickness Estimation from Geophysical Investigations on the Terminal Lobes of Belvedere Glacier (NW Italian Alps), Remote Sensing, 11, 805, https://doi.org/10.3390/rs11070805, 2019.

Colucci, R. R., Forte, E., Boccali, C., Dossi, M., Lanza, L., Pipan, M., and Guglielmin, M.: Evaluation of Internal Structure, Volume and Mass of Glacial Bodies by Integrated LiDAR and Ground Penetrating Radar Surveys: The Case Study of Canin Eastern Glacieret (Julian Alps, Italy), Surveys in Geophysics, 36, 231–252, https://doi.org/10.1007/s10712-014-9311-1, 2015.

Comiti, F., Mao, L., Penna, D., Dell'Agnese, A., Engel, M., Rathburn, S., and Cavalli, M.: Glacier melt runoff controls bedload transport in Alpine catchments, Earth and Planetary Science Letters, 520, 77–86, https://doi.org/10.1016/j.epsl.2019.05.031, 2019.

Cook, S. J., Swift, D. A., Kirkbride, M. P., Knight, P. G., and Waller, R. I.: The empirical basis for modelling glacial erosion rates, Nature Communications, 11, 759, https://doi.org/10.1038/s41467-020-14583-8, 2020.

Corte, E., Ajmar, A., Camporeale, C., Cina, A., Coviello, V., Giulio Tonolo, F., Godio, A., Macelloni, M. M., Tamea, S., and Vergnano, A.: Multitemporal characterization of a proglacial system: a multidisciplinary approach, Earth System Science Data, 16, 3283–3306, https://doi.org/10.5194/essd-16-3283-2024, 2024.

Crameri, F.: Scientific colour maps, https://doi.org/10.5281/ZENODO.1243862, language: en, 2021.

Cuffey, K. M.: J. Oerlemans. 2001. Glaciers and climate change: a meteorologist's view., Journal of Glaciology, 48, 173–173, https://doi.org/10.3189/172756502781831557, 2002.

Farinotti, D., Huss, M., Bauder, A., Funk, M., and Truffer, M.: A method to estimate the ice volume and ice-thickness distribution of alpine glaciers, Journal of Glaciology, 55, 422–430, https://doi.org/10.3189/002214309788816759, 2009.

Farinotti, D., Brinkerhoff, D. J., Clarke, G. K. C., Fürst, J. J., Frey, H., Gantayat, P., Gillet-Chaulet, F., Girard, C., Huss, M., Leclercq, P. W., Linsbauer, A., Machguth, H., Martin, C., Maussion, F., Morlighem, M., Mosbeux, C., Pandit, A., Portmann, A., Rabatel, A., Ramsankaran, R., Reerink, T. J., Sanchez, O., Stentoft, P. A., Singh Kumari, S., van Pelt, W. J. J., Anderson, B., Benham, T., Binder,

https://doi.org/10.5194/egusphere-2024-2569
Preprint. Discussion started: 25 September 2024

D., Dowdeswell, J. A., Fischer, A., Helfricht, K., Kutuzov, S., Lavrentiev, I., McNabb, R., Gudmundsson, G. H., Li, H., and Andreassen, L. M.: How accurate are estimates of glacier ice thickness? Results from ITMIX, the Ice Thickness Models Intercomparison eXperiment, The Cryosphere, 11, 949–970, https://doi.org/10.5194/tc-11-949-2017, 2017.

Favre, A.: Recherches Géologiques dans les Parties de la Savoie, du Piémont et de la Suisse voisines du Mont-Blanc. Avec un Atlas de 32 Planches, vol. 1, Paris V. Masson et Fils, Genève, https://doi.org/10.1017/S0016756800207711, publisher: Cambridge University Press, 1867.

Forte, E., Pipan, M., Francese, R., and Godio, A.: An overview of GPR investigation in the Italian Alps, First Break, 33, https://doi.org/10.3997/1365-2397.33.8.82011, 2015.

Forte, E., Santin, I., Ponti, S., Colucci, R. R., Gutgesell, P., and Guglielmin, M.: New insights in glaciers characterization by differential diagnosis integrating GPR and remote sensing techniques: A case study for the Eastern Gran Zebrù glacier (Central Alps), Remote Sensing of Environment, 267, 112 715, https://doi.org/10.1016/j.rse.2021.112715, 2021.

Frey, H., Machguth, H., Huss, M., Huggel, C., Bajracharya, S., Bolch, T., Kulkarni, A., Linsbauer, A., Salzmann, N., and Stoffel, M.: Estimating the volume of glaciers in the Himalayan–Karakoram region using different methods, The Cryosphere, 8, 2313–2333, https://doi.org/10.5194/tc-8-2313-2014, 2014.

Gizzi, M., Mondani, M., Taddia, G., Suozzi, E., and Lo Russo, S.: Aosta Valley Mountain Springs: A Preliminary Analysis for Understanding Variations in Water Resource Availability under Climate Change, Water, 14, 1004, https://doi.org/10.3390/w14071004, 2022.

Glen, J. W. and Paren, J. G.: The Electrical Properties of Snow and Ice, Journal of Glaciology, 15, 15–38, https://doi.org/10.3189/S0022143000034249, 1975.

Grab, M., Mattea, E., Bauder, A., Huss, M., Rabenstein, L., Hodel, E., Linsbauer, A., Langhammer, L., Schmid, L., Church, G., Hellmann, S., Délèze, K., Schaer, P., Lathion, P., Farinotti, D., and Maurer, H.: Ice thickness distribution of all Swiss glaciers based on extended ground-penetrating radar data and glaciological modeling, Journal of Glaciology, 67, 1074–1092, https://doi.org/10.1017/jog.2021.55, 2021.

Haeberli, W., Oerlemans, J., and Zemp, M.: The Future of Alpine Glaciers and Beyond, in: Oxford Research Encyclopedia of Climate Science, Oxford University Press, ISBN 978-0-19-022862-0, https://doi.org/10.1093/acrefore/9780190228620.013.769, 2019.

Huber, E. and Hans, G.: RGPR — An open-source package to process and visualize GPR data, in: 2018 17th International Conference on Ground Penetrating Radar (GPR), pp. 1–4, IEEE, Rapperswil, ISBN 978-1-5386-5777-5, https://doi.org/10.1109/ICGPR.2018.8441658, 2018.

Jol, H. M.: Ground penetrating radar theory and applications, Elsevier Science, Amsterdam, Netherlands, 1st edn., ISBN 978-0-08-095184-3, oCLC: 1078275154, 2009.

JPL, N.: NASADEM Merged DEM Global 1 arc second V001, https://doi.org/10.5067/MEASURES/NASADEM/NASADEM_HGT.001, 2020.

Karušs, J., Lamsters, K., Ješkins, J., Sobota, I., and Džeriņš, P.: UAV and GPR Data Integration in Glacier Geometry Reconstruction: A Case Study from Irenebreen, Svalbard, Remote Sensing, 14, 456, https://doi.org/10.3390/rs14030456, 2022.

Langhammer, L., Grab, M., Bauder, A., and Maurer, H.: Glacier thickness estimations of alpine glaciers using data and modeling constraints, The Cryosphere, 13, 2189–2202, https://doi.org/10.5194/tc-13-2189-2019, 2019a.

Langhammer, L., Rabenstein, L., Schmid, L., Bauder, A., Grab, M., Schaer, P., and Maurer, H.: Glacier bed surveying with helicopter-borne dual-polarization ground-penetrating radar, Journal of Glaciology, 65, 123–135, https://doi.org/10.1017/jog.2018.99, 2019b.

https://doi.org/10.5194/egusphere-2024-2569
Preprint. Discussion started: 25 September 2024

Langley, K., Lacroix, P., Hamran, S.-E., and Brandt, O.: Sources of backscatter at 5.3 GHz from a superimposed ice and firn area revealed by multi-frequency GPR and cores, Journal of Glaciology, 55, 373–383, https://doi.org/10.3189/002214309788608660, 2009.

Linsbauer, A., Paul, F., and Haeberli, W.: Modeling glacier thickness distribution and bed topography over entire mountain ranges with GlabTop: Application of a fast and robust approach: REGIONAL-SCALE MODELING OF GLACIER BEDS, Journal of Geophysical Research: Earth Surface, 117, https://doi.org/10.1029/2011JF002313, 2012.

Macelloni, M. M., Corte, E., Ajmar, A., Cina, A., Giulio Tonolo, F., Maschio, P. F., and Pisoni, I. N.: Multi-platform, Multi-scale and Multi-temporal 4D Glacier Monitoring. The Rutor Glacier Case Study, in: Geomatics for Green and Digital Transition, edited by Borgogno-Mondino, E. and Zamperlin, P., vol. 1651, pp. 392–404, Springer International Publishing, Cham, ISBN 978-3-031-17438-4 978-3-031-17439-1, https://doi.org/10.1007/978-3-031-17439-1_29, series Title: Communications in Computer and Information Science, 2022.

Maussion, F., Butenko, A., Champollion, N., Dusch, M., Eis, J., Fourteau, K., Gregor, P., Jarosch, A. H., Landmann, J., Oesterle, F., Recinos, B., Rothenpieler, T., Vlug, A., Wild, C. T., and Marzeion, B.: The Open Global Glacier Model (OGGM) v1.1, Geoscientific Model Development, 12, 909–931, https://doi.org/10.5194/gmd-12-909-2019, 2019.

Milner, A. M., Khamis, K., Battin, T. J., Brittain, J. E., Barrand, N. E., Füreder, L., Cauvy-Fraunié, S., Gíslason, G. M., Jacobsen, D., Hannah, D. M., Hodson, A. J., Hood, E., Lencioni, V., Ólafsson, J. S., Robinson, C. T., Tranter, M., and Brown, L. E.: Glacier shrinkage driving global changes in downstream systems, Proceedings of the National Academy of Sciences, 114, 9770–9778, https://doi.org/10.1073/pnas.1619807114, 2017.

Monti, R.: Recherches sur quelques lacs du Massif du Ruitor, 1, 120–167, https://archive.org/details/cbarchive_54671_recherchessurquelqueslacsdumas1906/mode/2up, 1906.

Orombelli, G.: The Ruitor glacier (Aosta Valley) during the Little Ice Age, Geografia Fisica e Dinamica Quaternaria, pp. 239–251, 2005.

Preller, C. D. R.: The Ruitor Glacier lakes (Piedmontese Alps), Scottish Geographical Magazine, 34, 330–342, https://doi.org/10.1080/14702541808554167, 1918.

QGIS-Development-Team: QGIS Geographic Information System, https://www.qgis.org, 2024.

Reinardy, B. T. I., Booth, A. D., Hughes, A. L. C., Boston, C. M., Åkesson, H., Bakke, J., Nesje, A., Giesen, R. H., and Pearce, D. M.: Pervasive cold ice within a temperate glacier – implications for glacier thermal regimes, sediment transport and foreland geomorphology, The Cryosphere, 13, 827–843, https://doi.org/10.5194/tc-13-827-2019, 2019.

Rutishauser, A., Maurer, H., and Bauder, A.: Helicopter-borne ground-penetrating radar investigations on temperate alpine glaciers: A comparison of different systems and their abilities for bedrock mapping, Geophysics, 81, WA119–WA129, https://doi.org/10.1190/geo2015-0144.1, 2016.

Sacco, F.: Il ghiacciaio ed i laghi del Ruitor, 36, 1–36, https://www.socgeol.info/it/benvenuti/, 1917.

Sandmeier, K.: REFLEXW Version 7.0-program for the Processing of Seismic, Acoustic or Electromagnetic Reflection, Refraction and Transmission Data, User's Manual, 578, https://www.sandmeier-geo.de/guides-and-videos.html, 2012.

Santin, I., Forte, E., Nicora, M., Ponti, S., and Guglielmin, M.: Where does a glacier end? Integrated geophysical, geomorphological and photogrammetric measurements to image geometry and ice facies distribution, Catena, 225, 107 016, https://doi.org/10.1016/j.catena.2023.107016, 2023.

Schwanghart, W. and Scherler, D.: Short Communication: TopoToolbox 2 – MATLAB-based software for topographic analysis and modeling in Earth surface sciences, Earth Surface Dynamics, 2, 1–7, https://doi.org/10.5194/esurf-2-1-2014, 2014.

Sober, E.: Ockham's razors: a user's manual, Cambridge University Press, Cambridge, ISBN 978-1-107-06849-0 978-1-107-69253-4, 2015.

https://doi.org/10.5194/egusphere-2024-2569
Preprint. Discussion started: 25 September 2024

Strigaro, D., Moretti, M., Mattavelli, M., Frigerio, I., Amicis, M. D., and Maggi, V.: A GRASS GIS module to obtain an estimation of glacier behavior under climate change: A pilot study on Italian glacier, Computers & Geosciences, 94, 68–76, https://doi.org/10.1016/j.cageo.2016.06.009, 2016.

Suter, S., Laternser, M., Haeberli, W., Frauenfelder, R., and Hoelzle, M.: Cold firn and ice of high-altitude glaciers in the Alps: measurements and distribution modelling, Journal of Glaciology, 47, 85–96, https://doi.org/10.3189/172756501781832566, 2001.

Urbini, S., Bianchi-Fasani, G., Mazzanti, P., Rocca, A., Vittuari, L., Zanutta, A., Girelli, V. A., Serafini, M., Zirizzotti, A., and Frezzotti, M.: Multi-Temporal Investigation of the Boulder Clay Glacier and Northern Foothills (Victoria Land, Antarctica) by Integrated Surveying Techniques, Remote Sensing, 11, 1501, https://doi.org/10.3390/rs11121501, 2019.

Vergnano, A., Oggeri, C., and Godio, A.: Geophysical-geotechnical methodology for assessing the spatial distribution of glacio-lacustrine sediments: the case history of Lake Seracchi, Earth Surface Processes and Landforms, p. esp.5555, https://doi.org/10.1002/esp.5555, 2023.

Viani, C., Machguth, H., Huggel, C., Perotti, L., and Giardino, M.: Detecting glacier-bed overdeepenings for glaciers in the Western Italian Alps using the GlabTop2 model: the test site of the Rutor Glacier, Aosta Valley, in: EGU General Assembly Conference Abstracts, pp. EPSC2016–13 607, 2016.

Viani, C., Machguth, H., Huggel, C., Godio, A., Franco, D., Perotti, L., and Giardino, M.: Potential future lakes from continued glacier shrinkage in the Aosta Valley Region (Western Alps, Italy), Geomorphology, 355, 107 068, https://doi.org/10.1016/j.geomorph.2020.107068, 2020.

Villa, F., De Amicis, M., and Maggi, V.: GIS analysis of Rutor Glacier (Aosta Valley, Italy) volume and terminus variations, Geografia Fisica e Dinamica Quaternaria, 30, 87–95, www.scopus.com, 2007.

Villa, F., Tamburini, A., Deamicis, M., Sironi, S., Maggi, V., and Rossi, G.: Volume decrease of Rutor Glacier (Western Italian Alps) since little ice age: A quantitative approach combining GPR, GPS and cartography, Geografia Fisica e Dinamica Quaternaria, 31, 63–70, www.scopus.com, 2008.

Weertman, J.: Mechanism for the Formation of Inner Moraines Found Near the Edge of Cold Ice Caps and Ice sheets, Journal of Glaciology, 3, 965–978, https://doi.org/10.3189/S0022143000017378, 1961.

https://doi.org/10.5194/egusphere-2024-2569
Preprint. Discussion started: 25 September 2024

Appendix A: Appendix - GPR Sections

This appendix is devoted to all the GPR sections analyzed in this work, to show the interested reader what the data looked like, which were the difficulties, and in which cases the three models' predictions were useful in avoiding clear misinterpretations. In any case, the interpretation subjectivity is high, and analyzing the openly available GPR dataset with specialistic software is advised. The first 5 figures represent the 5 GPR sections of the 2012 heli-based survey; the last figure is the merging of all (subsequent) sections of the 2022 ground-based survey. See Figure 6 for the location of the GPR sections. The three models are pictured in with different lines.

https://doi.org/10.5194/egusphere-2024-2569
Preprint. Discussion started: 25 September 2024

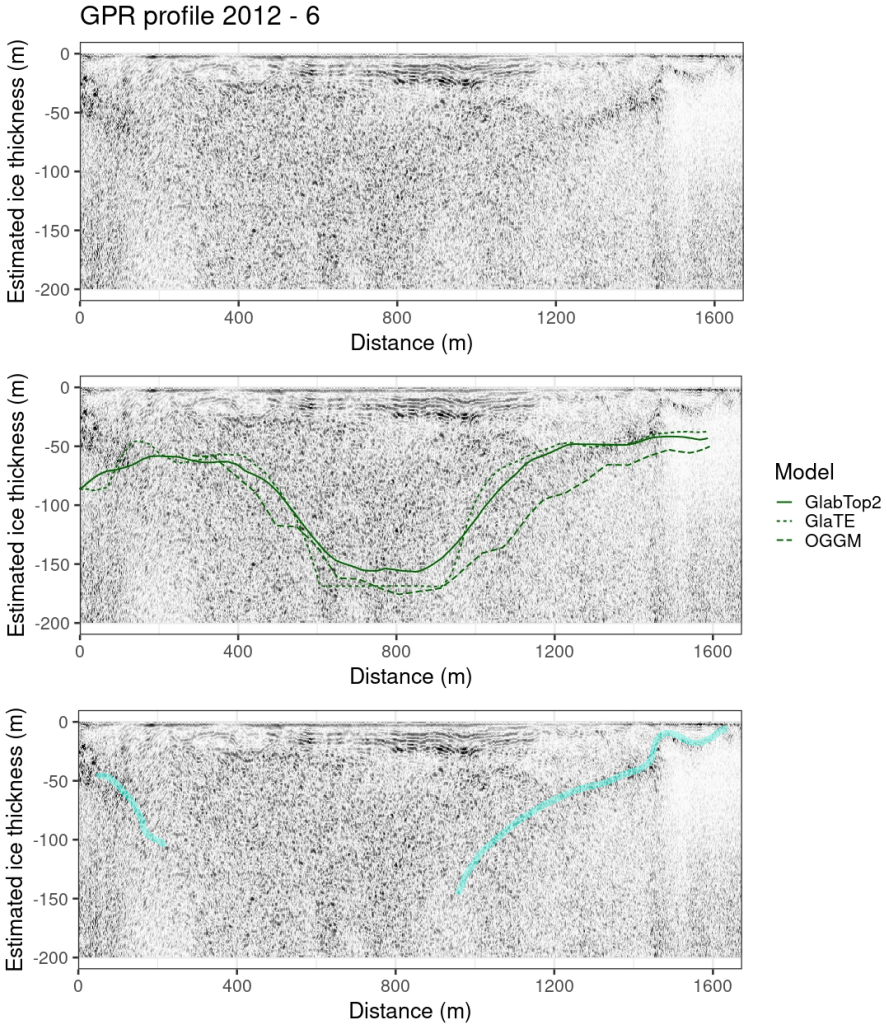

Figure A1. GPR section 2012 - 6. This section is situated at the top of the glacier, and in its central part (500-1000 m of Distance coordinate) the three models estimate an overdeepening of over 150 m. The GPR reflections are reasonably clear until 50-70 m of depth. In the right part of the picture, the models follow closely the GPR reflections; however, they are quite imprecise just near the outline, where they do not draw correctly the bedrock shape where the ice is very thin. Based on the estimates of the models, the analyst did not pick the sparse reflections at 25-30 m depth as an ice-bedrock interface but acknowledged that, in the right part, the deepening reflections continue to go deeper leftward until around the center of the image.

https://doi.org/10.5194/egusphere-2024-2569
Preprint. Discussion started: 25 September 2024

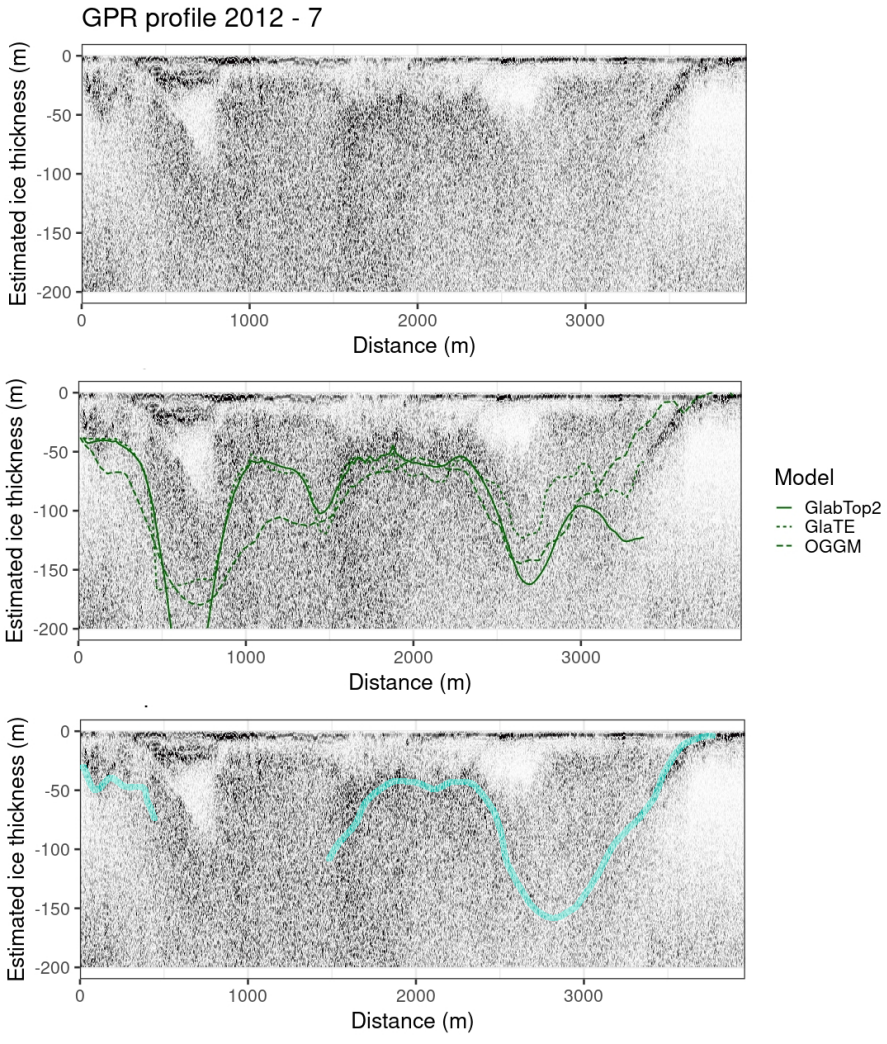

Figure A2. GPR section 2012 - 7. This section was already shown and discussed in Figure 5, but it is possible to add a consideration on the steep overdeepening "seen" by the GlabTop2 model. The creation of deep overdeepenings was recognized to be an artifact of such models, especially when using a too-fine input DEM [Maurer and Grab, personal communication]. Also, the other models estimate a high ice thickness at that point, but they seem more realistic. Unfortunately, the GPR was of little help in that region.

https://doi.org/10.5194/egusphere-2024-2569
Preprint. Discussion started: 25 September 2024

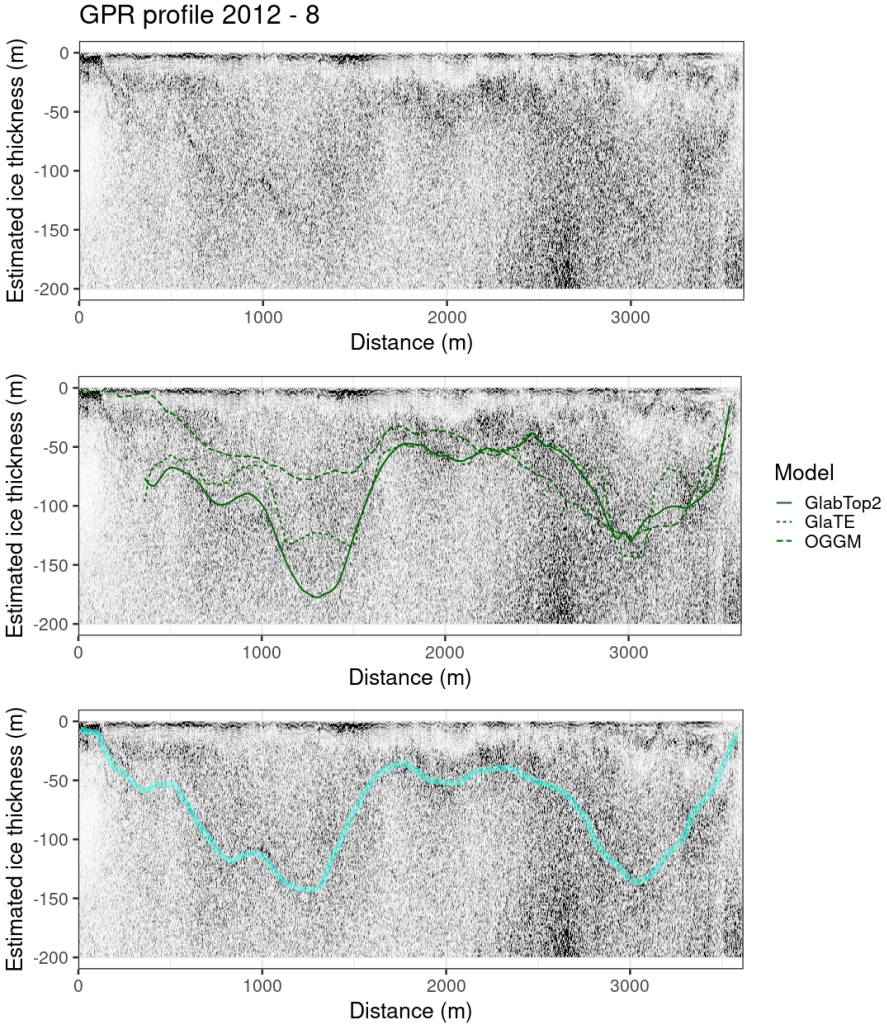

Figure A3. GPR section 2012 - 8. This GPR section was probably the most clear of the dataset. The ice-bedrock reflector can be followed in almost all the images to great depths, although the clarity is far from ideal. This section can be considered proof that the models are capable of doing reasonable estimates of the ice thickness in Rutor glacier, especially the GlabTop2 and the GlaTE, while OGGM performed poorly in the left part of the image. In the left part of the image, which corresponds to the Eastern tongue, the models go to 0 because they were cut with the 2021 outline. From 2012 to 2021, the glacier experienced a notable retreat. in the Eastern tongue.

https://doi.org/10.5194/egusphere-2024-2569
Preprint. Discussion started: 25 September 2024

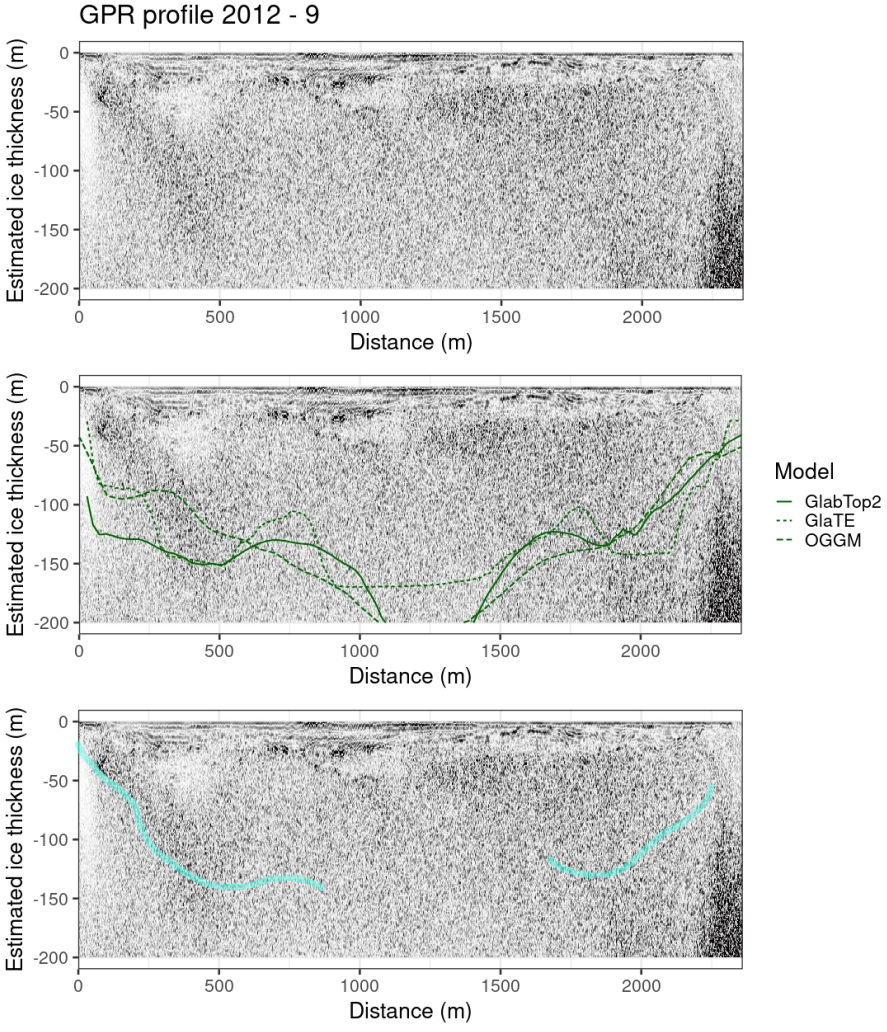

Figure A4. GPR section 2012 - 9. This GPR section was probably the least clear. Its path runs along the elongated overdeepening of the top of the glacier (Figure 6). In the left part of the picture, the reflections deepen very fast, and this is reproduced also by the models, but after that, it was impossible to retrieve any other reflections attributable to the ice-bedrock interface. The role of the models, in this case, was very important, to avoid thinking that the darker reflections seen in the center-right part of the image at 30-50 m depth are the bedrock interface, while probably it is due to the higher meltwater content, or debris (Forte et al., 2021).

https://doi.org/10.5194/egusphere-2024-2569
Preprint. Discussion started: 25 September 2024

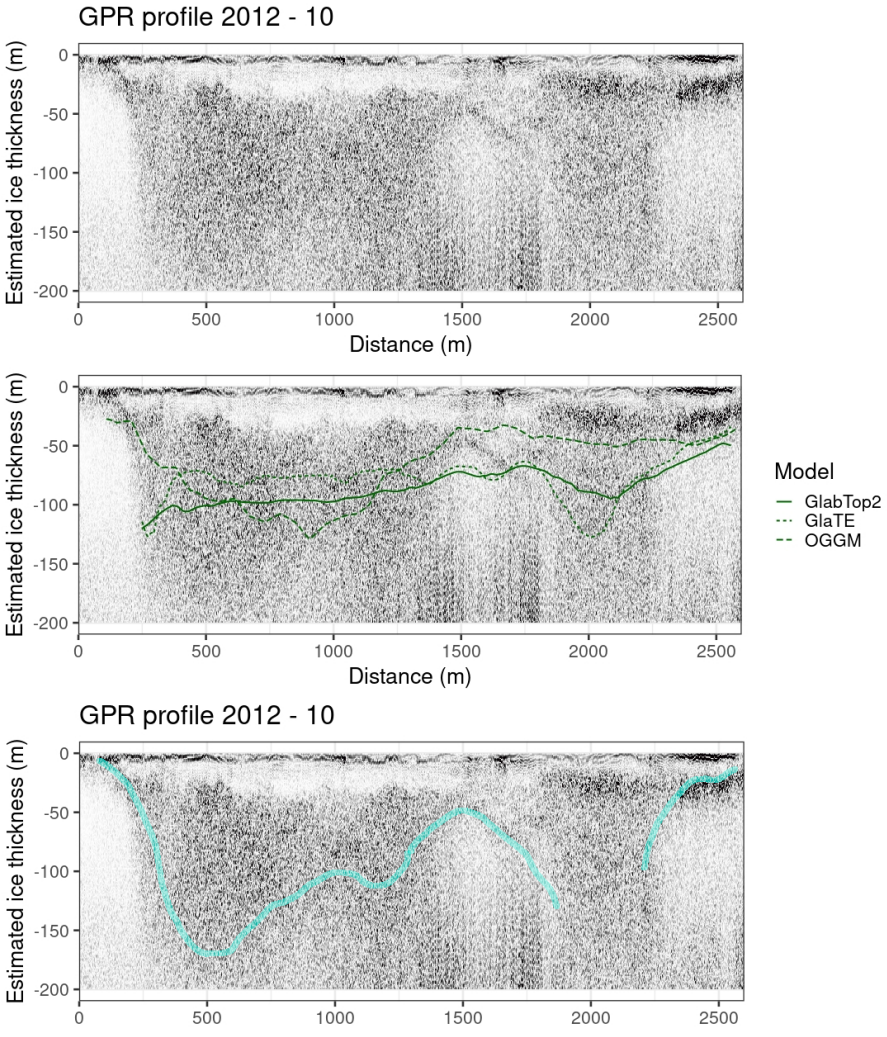

Figure A5. GPR section 2012 - 10. This GPR section was generally clear in the right part of the image and also showed consistency between GPR and models. All the profile has an interface around 30-40 m interpreted as meltwater or debris (Forte et al., 2021). The left part of the picture was more problematic, because the GPR, although not clear, seems to suggest a deeper bedrock interface than the models. Probably, this is due to a very problematic location of this survey line, possibly running along a very high-sloping bedrock (Figure 6). Such high-slope bedrock areas are known to disrupt GPR measurements and they could be common near the overdeepenings of Rutor glacier since they are also evidenced in many locations in the proglacial zone (which was formerly occupied by ice during the glaciations).

https://doi.org/10.5194/egusphere-2024-2569
Preprint. Discussion started: 25 September 2024

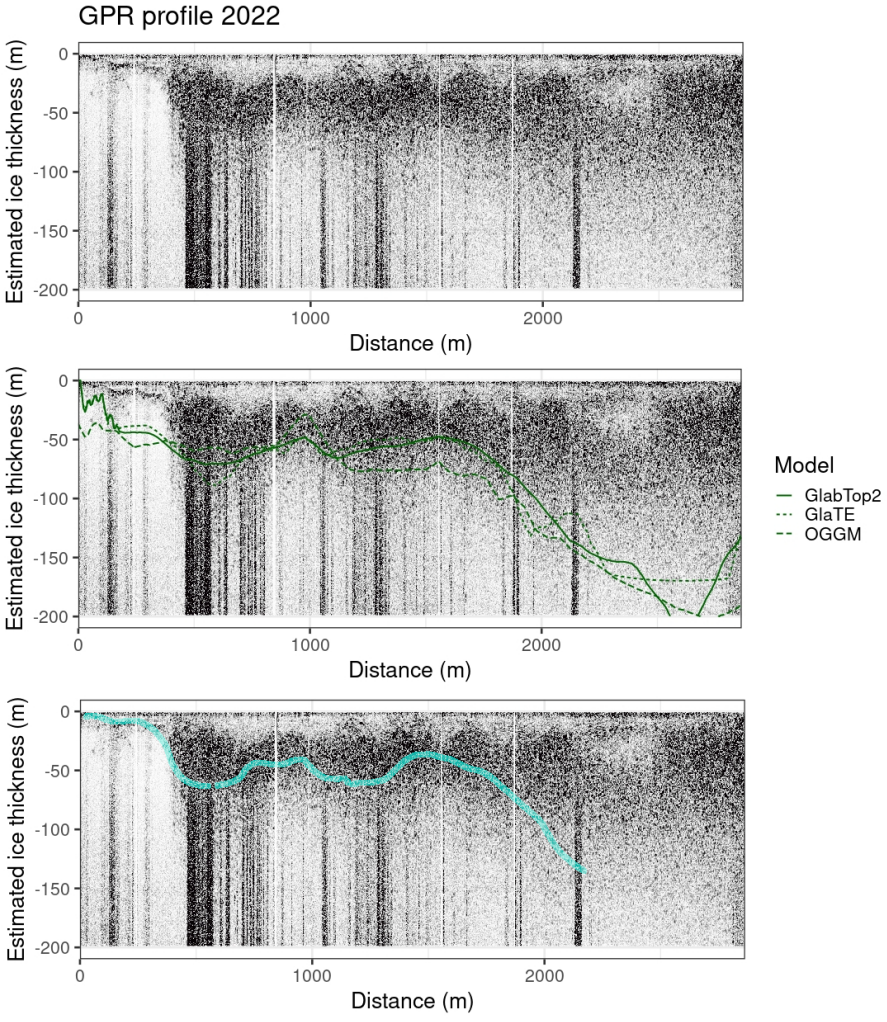

Figure A6. GPR section 2022. This GPR section was acquired with an antenna (40 MHz) different from that used for the previous sections shown. It also was ground-based and not helicopter-based. Notwithstanding the lower frequency and being ground-based, the GPR reflections were not particularly clearer, showing a physical limit of the technology in the presence of widespread meltwater inside ice or debris (Forte et al., 2021). The models did not perform well near the outline, as observed quite everywhere. However, probably they offer a reasonable estimate of the bedrock interface in all the left-central part of the image. The right part seems more problematic because the GPR signal is completely lost, however, its greater depth is supported by the GPR signal texture: compare e.g. the image at 100 m depth at Distance = 1000 m and = 2500 m. At distance = 2500 m, the image shows a granular texture similar to where there is ice and meltwater, while at Distance = 1000 m the texture is transparent. Similar considerations were used to interpret the GPR sections by (Forte et al., 2021).